Correlation effects in the total energy, the bulk modulus, and the lattice constant of a transition metal: Combined local-density approximation and dynamical mean-field theory applied to Ni and Mn

I. Di Marco,[1,*] J. Minár,[2] S. Chadov,[2,3] M. I. Katsnelson,[1] H. Ebert,[2] and A. I. Lichtenstein[4]
[1]*Institute for Molecules and Materials, Radboud University of Nijmegen, NL-6525 ED Nijmegen, The Netherlands*
[2]*Department Chemie und Biochemie, Physikalische Chemie, Ludwig-Maximilians Universität München, D-81377 München, Germany*
[3]*Institut für Anorganische und Analytische Chemie, Johannes-Gutenberg Universität Mainz, 55128 Mainz, Germany*
[4]*Institute of Theoretical Physics, University of Hamburg, 20355 Hamburg, Germany*
(Received 27 September 2008; revised manuscript received 1 January 2009; published 16 March 2009)

We present an accurate implementation of total-energy calculations into the local-density approximation plus dynamical mean-field theory (LDA+DMFT) method. The electronic structure problem is solved through the full-potential linear muffin-tin orbital and Korringa-Kohn-Rostoker methods with a perturbative solver for the effective impurity suitable for moderately correlated systems. We have tested the method in detail for the case of Ni, and investigated the sensitivity of the results to the computational scheme and to the complete self-consistency. It is demonstrated that the LDA+DMFT method can resolve a long-standing controversy between the LDA/generalized gradient approximation density-functional approach and experiment for equilibrium lattice constant and bulk modulus of Mn.

DOI: 10.1103/PhysRevB.79.115111 PACS number(s): 71.15.Nc, 71.20.Be, 71.27.+a

I. INTRODUCTION

The state-of-the-art technique for calculating the electronic structure of materials is density-functional theory[1,2] (DFT) in its local-density approximation (LDA). However, despite numerous impressive successes, it faces serious difficulties for strongly correlated systems such as Mott insulators, heavy fermion systems, high-temperature superconductors, itinerant electron magnets, and many others. Some of these difficulties were overcame by merging LDA-based first-principles electronic structure calculations with the dynamical mean-field theory (the LDA+DMFT approach;[3,4] for review see Refs. 5–8). Most of the works done by this method deal with spectral properties of strongly correlated systems. At the same time, correlation effects are sometimes of crucial importance to describe also cohesive energy, equilibrium lattice constant, and bulk modulus, as demonstrated for the cases of plutonium[9,10] and cerium.[11,12] After these first attempts, the need of more systematic implementations and investigation of the numerical problems related to total-energy evaluation in the LDA+DMFT scheme arose. Recently Pourovskii *et al.*[13] have presented an interesting comparison between the correlation effects in the basic DMFT cycle (convergence in the local self-energy) and in the fully self-consistent DMFT cycle (convergence in the local self-energy and in the electron density). Two test cases have been studied with their implementation: the γ phase of metallic cerium and the Mott insulator Ce_2O_3. Both of them are close-packed *f*-electron systems, and they can be correctly described through the atomic sphere approximation within the linear muffin-tin orbital method (ASA-LMTO) and through the Hubbard-I approximation[4] for the self-energy of the local problem.

Up to now all the LDA+DMFT studies of the ground-state properties of strongly correlated systems concerned materials with rather localized *f* electrons. Here, we are interested in materials where the correlation effects are less dramatic and where the failures of the density-functional theory pertain only to some specific properties. The late transition metals Mn, Fe, Co, and Ni are correlated systems, and the LDA+DMFT approach was successfully applied to describe their spectral properties[14–22] as well as their magnetic properties.[17,23] In particular, the DMFT was implemented into full-potential Korringa-Kohn-Rostoker method (FP-KKR) (Ref. 19) and full-potential linear muffin-tin orbital method (FP-LMTO) (Ref. 22) to allow corresponding studies.

In the present paper we extend the previous implementations to calculate the total energy of the electronic system within the LDA+DMFT scheme, following the formalism of the spectral density-functional theory.[6] Then these implementations are applied to the study of the total energy and the ground-state properties of two 3*d* transition metals. First, we present computational results for Ni which plays the role of "drosophila fly" for the LDA+DMFT method and where the most detailed comparison of the theory with experiment was done.[20,21] After calculations of photoemission, optical and magneto-optical spectra, magnetization, magnetic susceptibility, orbital magnetic moments, and bulk and surface spectral densities (see previous works cited above), the present calculation of cohesive energy, equilibrium lattice constant, and bulk modulus completes its basic physical description within the LDA+DMFT approach.

Comparing the results of the full-potential KKR and LMTO calculations, we address the question about sensitivity of the LDA+DMFT description to the band-structure method used. This is nontrivial since different methods use different basis sets which are truncated in any real calculations. We have found that actually the results are very close which support its reliability. While correlation effects in ground-state properties of Ni are quite small, they are accurately described within our scheme which confirms the usefulness of the LDA+DMFT for not only strongly correlated but also for moderately correlated systems. We have checked

also the importance of the full charge self-consistency and found that in the case of Ni these effects are not very essential.

Then, we consider the case of Mn where, among all transition metals, the largest discrepancy between the LDA or generalized gradient approximation (GGA) predictions for the lattice constant and bulk modulus, and the experimental data takes place[24–26] which is considered to be an indication of the strongest correlation effects among $3d$ metals.[18,27] We show that the LDA+DMFT method does allow us to solve this problem and to describe in a very satisfactory way the energetics of Mn.

II. FORMULATION OF THE PROBLEM

All the standard approaches for calculating the electronic structure of strongly correlated materials are based on the choice of a set of orbitals that are described not accurately enough in the standard DFT-LDA method which is supposed to be improved. We call them "correlated orbitals" and indicate with $|\mathbf{R},\xi\rangle$, where $\mathbf{R}$ is the vector specifying the Bravais lattice site and the ξ is an index that enumerates the orbitals within the unit cell of the crystal. The choice of $\{|\mathbf{R},\xi\rangle\}$ is dictated by physical motivations for the problem under consideration and always implies some degree of arbitrariness (see the discussion below). Usually the correlated orbitals are derived from d or f atomic states and the index ξ stands for the atomic quantum numbers l, m, and σ. Natural choices can be linear muffin-tin orbitals[10] or Wannier functions.[28,29] Apart from the atomic states, hybridized orbitals can also be chosen depending on the problem. For example, in the transition-metal oxides the crystal field splits the LDA bands into two distinct groups, well separated in energy and suitable to be determined through downfolding of the original problem via the order-N muffin-tin orbital (NMTO) approach.[30]

After having decided the set $\{|\mathbf{R},\xi\rangle\}$, we correct the standard DFT-LDA Hamiltonian with an additional Hubbard interaction term[6] that explicitly describes the local Coulomb repulsion U for the orbitals in the set:

$$H = H_{\mathrm{LDA}} + \frac{1}{2}\sum_{\mathbf{R}} \sum_{\xi_1,\xi_2,\xi_3,\xi_4} U_{\xi_1,\xi_2,\xi_3,\xi_4} c^{\dagger}_{\mathbf{R},\xi_1} c^{\dagger}_{\mathbf{R},\xi_2} c_{\mathbf{R},\xi_4} c_{\mathbf{R},\xi_3}. \tag{1}$$

This is the so-called LDA+U Hamiltonian and an important remark has to be made concerning the meaning of the matrix elements $U_{\xi_1,\xi_2,\xi_3,\xi_4}$. We should not think of them as generic matrix elements of the bare Coulomb repulsion but more as the matrix elements of an effective interaction introduced to give the correct description of the low-energy excitations (to describe broader energy scales, the U term should be, in general, energy dependent[31]). In these terms we have to consider the LDA+U Hamiltonian as being derived from completely *ab initio* density-functional approach. While in principle this is possible through many methods, e.g., constrained density-functional theory[32,33] and extraction from GW results,[31] it is a common practice to evaluate the matrix elements $U_{\xi_1,\xi_2,\xi_3,\xi_4}$ using semiempirical procedures.[14,34] This may seem to be inadequate since the strength of the effective Coulomb interaction should depend on the set of correlated orbitals, being strictly connected to a mapping of the original electronic Hamiltonian into Eq. (1); however if the orbitals $\{|\mathbf{R},\xi\rangle\}$ are chosen appropriately, the results are quite stable with respect to this ambiguity, as it was first noticed for the LDA+U method.[35]

If the correlated orbitals are atomiclike ones (with the quantum numbers l, m, and σ), we can express[35] the Coulomb parameters in terms of Slater integrals F^n such as

$$U_{\xi_1,\xi_2,\xi_3,\xi_4} = \sum_{n=0}^{2l} a_n(\xi_1,\xi_3,\xi_2,\xi_4) F^n, \tag{2}$$

with the coefficients a_n defined as

$$a_n(\xi_1,\xi_3,\xi_2,\xi_4) = \frac{4\pi}{2n+1} \sum_{q=-n}^{+n} \langle \xi_1 | Y_{nq} | \xi_3 \rangle \langle \xi_2 | Y^*_{nq} | \xi_4 \rangle, \tag{3}$$

where the terms $\langle \xi_1 | Y_{nq} | \xi_3 \rangle$ and $\langle \xi_2 | Y^*_{nq} | \xi_4 \rangle$ are integrals over products of three spherical harmonics. In the rest of the paper we are interested in $3d$ electrons; therefore we can limit our discussion to these. For d electrons there are only three Slater parameters (F^0, F^2, and F^4), and they can be easily linked to the Coulomb parameters U and J as[35]

$$U = F^0, \quad J = \frac{F^2 + F^4}{14}. \tag{4}$$

The ratio F^4/F^2 is assumed to correspond to the atomic value and for $3d$ electrons it is approximately equal to 0.625. In the rest of the paper we will use the two real values U and J to specify the Coulomb matrix elements.

III. DYNAMICAL MEAN-FIELD THEORY

In this section we present the basic equations of the dynamical mean-field theory. To keep the formulation as general as possible and to avoid references to any DFT-LDA method, all the equations of this section are written as equations for operators, unless differently stated.

The LDA+U Hamiltonian defines an "effective" Hubbard model, and its solution represents a complicated many-body problem. The strategy of the spectral density-functional theory[6] is the same as DFT or Baym-Kadanoff theory (or more generally of every Weiss mean-field theory): we specify a main observable quantity and we map the original system into a system with less degrees of freedom under the condition of conserving the expectation value of the main observable. In DFT and Baym-Kadanoff theory, the main observables are, respectively, the total electron density $\rho(\mathbf{r})$ and the one-electron Green's function $\hat{G}(z)$, namely,

$$\hat{G}(z) = [(z-\mu)\hat{\mathbf{1}} - \hat{h}_{\mathrm{LDA}} - \hat{\Sigma}(z)]^{-1}, \tag{5}$$

where z is the energy in the complex plane, μ is the chemical potential, h_{LDA} plays the role of the unperturbed Hamiltonian ("hopping"), and $\hat{\Sigma}(z)$ is the self-energy operator, which in many-body theory reproduces the effects of the interactions. In spectral density-functional theory the main observable is the local Green's function at the site $\mathbf{R}$:

$$\hat{G}_{\mathbf{R}}(z) = \hat{P}_{\mathbf{R}}\hat{G}(z)\hat{P}_{\mathbf{R}}, \tag{6}$$

where

$$\hat{P}_{\mathbf{R}} = \sum_{\xi} |\mathbf{R},\xi\rangle\langle\mathbf{R},\xi| \tag{7}$$

is the projection operator to the correlated subspace belonging to site $\mathbf{R}$.

As in density-functional theory, where we make approximations as LDA or GGA, in the framework of the spectral density-functional theory, the corresponding approximation is the dynamical mean-field theory. In the DMFT the self-energy is considered to be purely local. In terms of matrix elements on the correlated orbitals at the two sites $\mathbf{R}_1$ and $\mathbf{R}_2$, this means that

$$\langle \mathbf{R}_1,\xi_1|\hat{\Sigma}(z)|\mathbf{R}_2,\xi_2\rangle = \delta_{\mathbf{R}_1,\mathbf{R}_2}\langle\xi_1|\hat{\Sigma}_{\mathbf{R}_1}(z)|\xi_2\rangle. \tag{8}$$

The assumption of a purely local self-energy $\hat{\Sigma}_{\mathbf{R}}(z)$ allows us to focus only on the single lattice site $\mathbf{R}$. Consequently we can replace all the other sites of the lattice with a self-consistent electronic bath (or "dynamical mean-field") $\hat{\mathcal{G}}_0^{-1}(\mathbf{R},z)$, whose role is analogous to the Weiss mean-field used in statistical mechanics. What we have obtained is a problem of an atomic site embedded into the fermionic bath: in many-body physics this system is known as multiband Anderson impurity model. While we have not obtained a Hamiltonian that describes the mapping system, we can easily write down the effective action S:

$$S = -\int\int d\tau d\tau' \sum_{\xi_1,\xi_2} c^{\dagger}_{\xi_1}(\tau')[\mathcal{G}_0^{-1}]_{\xi_1,\xi_2}(\tau-\tau')c_{\xi_2}(\tau) + \frac{1}{2}\int d\tau \sum_{\xi_1,\xi_2,\xi_3,\xi_4} c^{\dagger}_{\xi_1}(\tau)c^{\dagger}_{\xi_2}(\tau)U_{\xi_1,\xi_2,\xi_3,\xi_4}c_{\xi_4}(\tau)c_{\xi_3}(\tau), \tag{9}$$

where τ is the imaginary time for the finite-temperature many-body formalism and the integrals have to be intended from 0 to $\beta=1/K_BT$. Notice that this action must be formulated directly for the local problem, leading to the matrix elements of the operator $\hat{\mathcal{G}}_0^{-1}$ on the set of the correlated orbitals. Furthermore for sake of visualization we omitted the subscript $\mathbf{R}$ in the bath Green's function, and in the creation and annihilation operators. Now the problem is fully determined and the impurity Green's function $\hat{G}_{\mathrm{imp}}(z)$ arises from the dynamics described by S through statistical average. Using the inverse Dyson equation it is possible to obtain an explicit expression for the self-energy operator from the fictitious impurity problem:

$$\hat{\Sigma}_{\mathbf{R}}(z) = \hat{\mathcal{G}}_0^{-1}(\mathbf{R},z) - \hat{G}^{-1}_{\mathrm{imp}}(z). \tag{10}$$

For a more detailed and rigorous description of the DMFT equations, which is beyond the scope of this paper, the authors redirect the reader to one of the excellent reviews of Ref. 6 and 7.

The Anderson impurity model has been widely studied in the many-body literature and its solution can be obtained through many different techniques, usually named "solvers" in the DMFT community. At the present time no solver has succeeded in becoming the "standard approach" of the LDA+DMFT scheme but the technique to be used is every time decided with respect to the strength of the correlations and the degree of accuracy desired. In the case of systematic simulations, as, for example, the total-energy calculations reported in this paper, another important factor to consider is the numerical efficiency. In both the implementations of the LDA+DMFT scheme discussed here, the spin-orbit spin-polarized T-matrix fluctuation-exchange (SPTF) (Refs. 15 and 36) solver has been used. SPTF is reliable and efficient for moderate strength of the correlations ($U \lesssim W/2$, where W is the bandwidth of the localized orbitals), and has been successfully and intensively applied to various systems as $3d$ metals,[14,15,19–23] half-metallic ferromagnets,[8] and actinides compounds.[36]

Once the effective impurity problem has been solved and a self-energy $\hat{\Sigma}_{\mathbf{R}}(z)$ has been obtained, there is an apparent change in the number of particles so that the chemical potential μ has to be updated and a new Green's function arises from Eq. (5). Furthermore a new electronic bath $\hat{\mathcal{G}}_0^{-1}(\mathbf{R},z)$ is defined through the inverse Dyson equation:

$$\hat{\mathcal{G}}_0^{-1}(\mathbf{R},z) = \hat{G}^{-1}_{\mathbf{R}}(z) + \hat{\Sigma}_{\mathbf{R}}(z). \tag{11}$$

Now we can iterate the procedure described above until convergence of the self-energy and the number of particles (or chemical potential). This is the basic DMFT cycle and is schematically reproduced in Fig. 1. From the same figure, we can also notice that, if the correlations are strong, the differences in the population of the Kohn-Sham orbitals lead to a new electron density $\rho(\mathbf{r})$. In this "full self-consistent cycle" also, the convergence of $\rho(\mathbf{r})$ has to be reached. In the present paper two implementations of the LDA+DMFT scheme are used: the first one works only within the basic DMFT cycle while the other one uses the fully self-consistent cycle. There are mainly two reasons why we have compared these two different implementations. First of all we want to study $3d$ states in bulk transition metals: they are not extremely localized so that their bandwidth is always bigger than the values of the effective Coulomb repulsions ($U \lesssim W$). Then we can reasonably suppose that the changes in the electron density are small, and a measure of this is given by the comparison of the two different codes. In second place one of the aims of our study is to investigate which numerical precision can be obtained for the LDA+DMFT scheme, also in comparison to the modern DFT packages so as to allow reliable calculation of sensitive quantities such as equilibrium atomic volume and bulk modulus. With respect to this issue, we should stress that implementing full self-consistency over the charge density is a very delicate task that can bring additional numerical errors. Moreover the computational effort can rise considerably, limiting the applications of the LDA+DMFT scheme to systems with a few atoms per unit cell.

Before presenting the total-energy functional adopted in the LDA+DMFT scheme, a final remark has to be made. Since the LDA+U Hamiltonian is constructed with an addi-

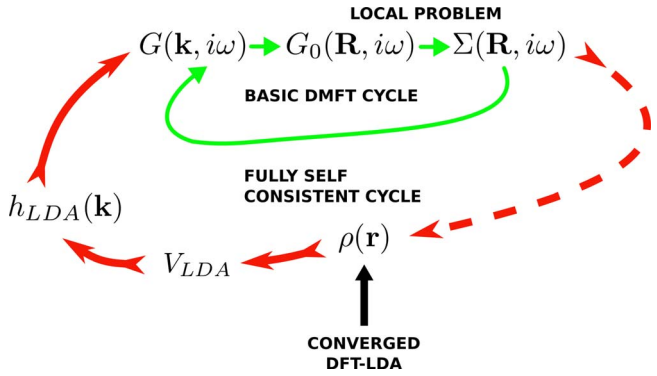

FIG. 1. (Color online) Schematic representation of the iterative procedure to follow in the LDA+DMFT scheme. As a first step the DFT-LDA problem is solved and a ground-state electron density $\rho(\mathbf{r})$ is obtained. From $\rho(\mathbf{r})$ we can extract the matrix elements of the single-particle LDA Hamiltonian, and then build the one-electron Green's function $G(\mathbf{k}, i\omega_n)$ at the Matsubara frequencies $i\omega_n$. Now the basic DMFT cycle starts: the Green's function $G(\mathbf{k}, i\omega_n)$ is projected onto the correlated orbitals, defining the bath Green's function $\mathcal{G}_0^{-1}(\mathbf{R}, i\omega_n)$ of the Anderson impurity model by means of Eq. (11). The solution of the local problem through one of the available solvers leads to a self-energy function $\Sigma_{\mathbf{R}}(i\omega_n)$. After a back projection to the LDA basis set, a new one-electron Green's function $G(\mathbf{k}, i\omega_n)$ and a new chemical potential μ are calculated. The procedure is repeated iteratively until convergence in the self-energy and the chemical potential. Once the convergence of the basic DMFT cycle has been reached, a new electron density $\rho(\mathbf{r})$ can be calculated from $G(\mathbf{k}, i\omega_n)$. This is the fully self-consistent cycle and should be continued until convergence in $\rho(\mathbf{r})$.

tional term that is already contained in the original electronic Hamiltonian, we have to remove from the self-energy those contributions already calculated in the LDA. Unfortunately, there is no way to establish exactly a correspondence between approximations within the density functional and the Green's function (Baym-Kadanoff) functional; then we have simply to "guess" which diagrammatic contributions are included and which ones are not. For treating metals the most common choice of the "double-counting" correction is the static part of the self-energy.[15,21] In the present paper we adopt the double counting of Ref. 23, i.e., we treat the static contribution to the self-energy as in the LDA+U method with around mean-field (AMF) double counting, while the other contributions to the self-energies become

$$\Sigma_{\xi_1,\xi_2}(z) = \Sigma_{\xi_1,\xi_2}(z) - \delta_{\xi_1,\xi_2}\langle\Sigma(0)\rangle, \tag{12}$$

where the matrix elements $\Sigma_{\xi_1,\xi_2}(z)$ stay for the matrix elements at right-hand side of Eq. (8), with the index $\mathbf{R}$ omitted due to the equivalence of the single sites. In Eq. (12) the average has to be determined over the orbital indices separately per spin channel. This choice is due to the fact that the LDA exchange-correlation potential is an orbitally averaged quantity and has proven to be very successful in describing the transition metals. In the rest of the paper the self-energy will always be considered as including the double-counting correction.

IV. TOTAL-ENERGY FUNCTIONAL

In the previous section we have presented the equations that define the LDA+DMFT scheme in terms of local problem and self-consistent bath. These equations can be obtained with many different techniques[37] but in perspective of total-energy calculations we have already adopted the point of view of the spectral density-functional theory of Savrasov and Kotliar. In a series of papers[6,10] they have introduced a functional of both the total electron density $\rho(\mathbf{r})$ and the local Green's function $G_{\mathbf{R}}(z)$ for the correlated orbitals. It is important to emphasize that these quantities are independent, in the sense that they cannot be reconstructed from each other. Furthermore notice that, in this framework, the arbitrariness of the basis set of the correlated orbitals is contained in $G_{\mathbf{R}}(z)$. Following standard methods of quantum-field theory, the functional is constructed, introducing source terms for $\rho(\mathbf{r})$ and $G_{\mathbf{R}}(z)$; then the variational procedure is applied to the functional with respect to these sources. Without presenting the mathematical details (see references above), we obtain the following expression for the zero-temperature limit of the total energy:

$$E = E_{\mathrm{LDA}}[\rho(\mathbf{r})] - {\sum_{\mathbf{k}\nu}}' \varepsilon_{\mathbf{k}\nu} + \mathrm{Tr}[\hat{H}_{\mathrm{LDA}}\hat{G}] + \langle\hat{H}_U\rangle, \tag{13}$$

where $\hat{H}_U$ indicates the two-particle term in LDA+U Hamiltonian (1), and the primed sum is over the occupied states. Here and in the following the symbol Tr indicates the one-electron trace for a generic representation and the sum over the Matsubara frequencies $i\omega$ for finite-temperature many-body formalism. We assume that the temperature effects can be taken into account only via summation over the Matsubara frequencies and, in the DFT part, only weak temperature dependence via the Fermi distribution function is taken into account.[38] This corresponds to neglecting the temperature dependence of the exchange-correlation potential and it is a standard procedure in electronic structure calculations of real materials. These effects are irrelevant for the cases under consideration where the main temperature dependence is due to spin fluctuations.[17]

We notice that the total energy within the LDA+DMFT scheme is not simply the expectation value of this Hamiltonian but it consists of several terms, in analogy to the expressions of the usual DFT. The first term $E_{\mathrm{LDA}}[\rho(\mathbf{r})]$ contains four different contributions, namely, the ones due to the external potential, the Hartree potential, the exchange-correlation potential, and the sum of the Kohn-Sham eigenvalues. However in the spectral density-functional theory, the Kohn-Sham eigenvalues should be reoccupied with respect to the description given by the total Green's function. Then we should remove the bare Kohn-Sham eigenvalues sum [second term of Eq. (13)] and substitute it with $\mathrm{Tr}[\hat{H}_{\mathrm{LDA}}\hat{G}]$ (third term). Moreover notice that $E_{\mathrm{LDA}}[\rho(\mathbf{r})]$ depends only on the total electron density so it does not need to be recalculated if the basic DMFT cycle is applied. In the case of the fully self-consistent cycle, the calculation is straightforward since it uses the same LDA-DFT machinery. This point will be analyzed in more details in the section concerning the FP-KKR implementation.

Finally we can evaluate $\langle \hat{H}_U \rangle$ through the so-called Galitskii-Migdal formula,[39,40] an elegant way to rewrite the expectation value of a two-particle operator in terms of a one-particle operator as the Green's function. This formula is based on the fact that for a Hamiltonian $\hat{H}=\hat{H}_0+\hat{H}_U$, i.e., the same form of Hamiltonian (1), the equation of motion of the Green's function states that

$$\left\langle \frac{\partial}{\partial \tau} \hat{G}(\tau) \right\rangle = \langle \hat{H}_0 \rangle + 2\langle \hat{H}_U \rangle, \tag{14}$$

where τ is the imaginary time for the finite-temperature formalism (the formulation for real times and $T=0$ is completely equivalent). Using the Fourier transform with respect to τ, we can move to the energy domain

$$\left\langle \frac{\partial}{\partial \tau} \hat{G}(\tau) \right\rangle = \mathrm{Tr}[\omega \hat{G}(\omega)]. \tag{15}$$

Furthermore from the definition of the Green's function $[\omega \hat{\mathbf{1}} - H_0 - \hat{\Sigma}(\omega)]\hat{G}(\omega) = \hat{\mathbf{1}}$, we can rewrite the expression above in terms of more manageable operators

$$\mathrm{Tr}[\omega \hat{G}(\omega)] = \mathrm{Tr}[\hat{\Sigma}(\omega)\hat{G}(\omega)] + \mathrm{Tr}[\hat{H}_0 \hat{G}(\omega)]. \tag{16}$$

Then the Galitskii-Migdal formula becomes

$$\langle \hat{H}_U \rangle = \frac{1}{2} \mathrm{Tr}[\hat{\Sigma}\hat{G}]. \tag{17}$$

Notice that in our notation the self-energy involved in the calculation of $\langle \hat{H}_U \rangle$ has been already corrected with the double-counting contribution through Eq. (12). This implies that no explicit double-counting term for the total energy has been added in functional (13), being already included in Eq. (17). A final remark is needed about the role of the double-counting term on the total energy in the LDA+DMFT scheme. Since the functional (13) depends on this *ansatz*, some of the previous implementations[13,41] have a slightly different form than the one proposed in the present paper. The reason is that those works address their studies to systems with stronger correlations ($U/W > 1$). Conversely we are focused on transition metals which are described in an excellent way by Eq. (12), as it has been illustrated at the end of the previous section and in the mentioned references.

V. IMPLEMENTATION IN FP-LMTO

We have implemented the total-energy algorithm of the previous section in the recently developed LDA+DMFT code,[22] based on the FP-LMTO method code presented in Ref. 42 and is well known to give accurate description of many solids within LDA. The full-potential character of the program makes it very attractive for open structures and surfaces, and in fact the first applications of our code were focused on these systems.[22] Furthermore the use of a small number of basis functions as used within the LMTO method is particularly efficient for calculating the Green's functions since they require inversions of a matrix in the LDA basis set for each Matsubara frequency and **k** point. While we do not want to give a complete survey of the equations involved in the FP-LMTO code, the study of the total-energy problem forced us to develop a more sophisticated method to calculate the number of electrons for the given chemical potential. In this implementation two basis sets are used: the already mentioned set of the correlated orbitals $\{|\mathbf{R},\xi\rangle\}$ and the set of the LDA basis functions $\{|\mathbf{k},\chi\rangle\}$. Conformingly to the standard LMTO notation, the index χ stands for the atom type in the unit cell, the atomic quantum numbers l, m, and σ, and the tail energy parameter κ, which describes the behavior of the basis functions in the interstitials between the muffin-tin spheres. As a result no explicit indices and sums will be considered for the spins (see Ref. 22 for further details).

The steps of the LDA+DMFT scheme that imply moving from the local problem to the lattice problem require transformations back and forth between these two basis sets. Furthermore we should mention that the set $\{|\mathbf{k},\chi\rangle\}$ is neither normalized nor orthogonal and then the basic algebraic operations involve an overlap matrix,

$$S(\mathbf{k})_{\chi_1,\chi_2} = \langle \mathbf{k},\chi_1 | \mathbf{k},\chi_2 \rangle, \tag{18}$$

and its inverse S^{-1} since the dual basis set of $\{|\mathbf{k},\chi\rangle\}$ does not coincide with the set itself. The number of electrons in the lattice problem is calculated with the LDA basis set and becomes

$$N = T\sum_{i\omega_n} \sum_{\mathbf{k}} \sum_{\chi_1,\chi_2} S(\mathbf{k})_{\chi_2,\chi_1} G(\mathbf{k},i\omega_n)_{\chi_1,\chi_2}, \tag{19}$$

where

$$G(\mathbf{k},i\omega_n)_{\chi_1,\chi_2} = \langle \mathbf{k},\chi_1 | \hat{G}(i\omega_n) | \mathbf{k},\chi_2 \rangle. \tag{20}$$

The sum over the Matsubara poles should include infinite negative and positive frequencies but obviously, in a computational scheme, the number of frequencies can only be finite and then a cutoff value $\omega_{\max}$ needs to be chosen. Unfortunately, as it is clear from definition (5), the Green's functions decay slowly with the energy and then a reliable determination of the number of particles would require a huge cutoff. There are two ways to reach this cutoff: increasing the number of Matsubara frequencies or increasing the spacing between them, proportional to the temperature T. None of them is a good solution. The former would imply too big numerical effort (there is an inversion of a matrix with the size of the LDA basis set for every Matsubara frequency and every **k** point) while the latter would lead us too far from the $T=0$ ground state. In Ref. 22 the problem of the long-decaying tails of the Green's function was solved in a rather rudimental way, given that the paper was focused on the spectral properties, which are not as sensitive as the ground-state properties to the numerical details. In the present paper, conversely, we follow the elegant procedure used in the LDA+DMFT calculations[6,13] and adapted it to our nonorthonormal basis set. The idea is to decompose the calculated Green's function (20) as

$$G(\mathbf{k},i\omega_n)_{\chi_1,\chi_2} = G(\mathbf{k},i\omega_n)^{\mathrm{num}}_{\chi_1,\chi_2} + G(\mathbf{k},i\omega_n)^{\mathrm{an}}_{\chi_1,\chi_2}, \tag{21}$$

where $G(\mathbf{k},i\omega_n)^{\mathrm{an}}_{\chi_1,\chi_2}$ is an analytical function that we chose to fit the high-frequency behavior of $G(\mathbf{k},i\omega_n)_{\chi_1,\chi_2}$:

$$\sum_{i\omega_n}^{(\omega_n>\omega_{\max})} [G(\mathbf{k},i\omega_n)_{\chi_1,\chi_2} - G(\mathbf{k},i\omega_n)^{\mathrm{an}}_{\chi_1,\chi_2}] = 0. \quad (22)$$

On the other hand the numerical part is defined as the difference between the calculated function and the analytical function,

$$G(\mathbf{k},i\omega_n)^{\mathrm{num}}_{\chi_1,\chi_2} \equiv G(\mathbf{k},i\omega_n)_{\chi_1,\chi_2} - G(\mathbf{k},i\omega_n)^{\mathrm{an}}_{\chi_1,\chi_2}, \quad (23)$$

and, if $G(\mathbf{k},i\omega_n)^{\mathrm{an}}_{\chi_1,\chi_2}$ has been chosen wisely, is negligible for $\omega_n > \omega_{\max}$.

The new problem is to determine G^{an}. Starting from definition (5), we can rewrite matrix element (20) as

$$G(\mathbf{k},i\omega_n)_{\chi_1,\chi_2} = \langle \mathbf{k},\chi_1 | [i\omega_n - \hat{A}_{\mathbf{k}}(i\omega_n)]^{-1} | \mathbf{k},\chi_2 \rangle, \quad (24)$$

where we have defined the new operator

$$\hat{A}_{\mathbf{k}}(i\omega_n) \equiv \mu\hat{\mathbf{1}} - \hat{h}_{\mathrm{LDA}} - \hat{\Sigma}(i\omega_n). \quad (25)$$

Let us consider $\hat{\Sigma}(i\omega_n)=0$ corresponding to the first iteration of the LDA+DMFT cycle. In this case operator (25) does not depend on the Matsubara frequencies and is Hermitian; consequently it has real eigenvalues $\lambda^{\mathbf{k}}_m$ and the eigenvectors $|X^{\mathbf{k}}_m\rangle$ can be chosen to form an orthonormal set. By expanding $\hat{A}_{\mathbf{k}}(i\omega_n)$ in its spectral representation, Eq. (21) becomes

$$G(\mathbf{k},i\omega_n)_{\chi_1,\chi_2} = G(\mathbf{k},i\omega_n)^{\mathrm{num}}_{\chi_1,\chi_2} + \sum_m \frac{\langle \mathbf{k},\chi_1 | X^{\mathbf{k}}_m \rangle \langle X^{\mathbf{k}}_m | \mathbf{k},\chi_2 \rangle}{i\omega_n - \lambda^{\mathbf{k}}_m}. \quad (26)$$

We have finally reduced the original sum to two terms that we can calculate with high precision. The numerical term is simply calculated as a sum for positive frequencies up to $\omega_{\max}$. The sum for negative frequencies is obtained using the symmetry of the Green's function

$$G(\mathbf{k},-i\omega_n)_{\chi_1,\chi_2} = [G(-\mathbf{k},i\omega_n)_{\chi_2,\chi_1}]^*. \quad (27)$$

The analytical term can be summed through standard many-body techniques:

$$\sum_{i\omega_n}\sum_m \frac{\langle \mathbf{k},\chi_1 | X^{\mathbf{k}}_m \rangle \langle X^{\mathbf{k}}_m | \mathbf{k},\chi_2 \rangle}{i\omega_n - \lambda^{\mathbf{k}}_m} = \sum_m \frac{\langle \mathbf{k},\chi_1 | X^{\mathbf{k}}_m \rangle \langle X^{\mathbf{k}}_m | \mathbf{k},\chi_2 \rangle}{1 + e^{\beta\lambda^{\mathbf{k}}_m}}. \quad (28)$$

In comparison with Ref. 13 finding eigenvalues and eigenvectors of $\hat{A}_{\mathbf{k}}$ is slightly more cumbersome here: due to the nonorthonormality of the basis set, we have to solve a generalized eigenvalue problem. However using the fact that the overlap matrix is positive definite, through Cholesky decomposition[43] of S, the problem can be reduced to a usual eigenvalue problem through a few algebraic operations.

When the DMFT self-energy assumes finite values, the operator $\hat{A}_{\mathbf{k}}(i\omega_n)$ is different at every Matsubara frequency, and then we need to use some approximation. Luckily in many-body theory the analytical properties of the self-energy operator are the same as for the Green's function. Therefore we can assume the following asymptotic behavior for high frequencies:[13]

$$\hat{\Sigma}(i\omega_n) \sim \hat{\Sigma}^{\mathrm{stat}} + \frac{\hat{\Sigma}^{\mathrm{asym}}}{i\omega}, \quad (29)$$

where $\hat{\Sigma}^{\mathrm{stat}}$ and $\hat{\Sigma}^{\mathrm{asym}}$ are obtained from the real and imaginary parts of $\hat{\Sigma}$ at the cutoff value $\omega_{\max}$. While a higher $\omega_{\max}$ will always give a better fit, the real part of the self-energy converges to $\hat{\Sigma}^{\mathrm{stat}}$ as $1/\omega^2$, and then we do not need a very high cutoff. Furthermore for our purposes of evaluating the frequency sum in Eq. (19), we can keep only the dominant term $\hat{\Sigma}^{\mathrm{stat}}$, and $\hat{\Sigma}^{\mathrm{asym}}$ turns to be unimportant. Again operator (25) becomes Hermitian and independent on the Matsubara frequencies so that the same procedure described above can be applied.

The implementation of this algorithm in the FP-LMTO code improved the precision in the determination of the number of particles by about two orders of magnitude in the worst cases (corresponding to a large number of LDA basis functions that increases the numerical error on the eigenvectors). The method used in Ref. 22 was rather similar to the one presented above but had a much simpler implementation. Instead of considering the asymptotic behavior of every Green's function in Eq. (19), the sum over the intermediate indices χ_1, χ_2, and $\mathbf{k}$ was done, and then the asymptotic behavior of the resulting function was considered. While this approximation can appear too crude, the precision on the number of particles is about 10^{-3} particles for every electron involved in the problem. On the other hand it was computationally very efficient since the generalized eigenvalue problem was reduced to the determination of a pure number.

After having improved the precision in the determination of the number of particles, we can pass to the implementation of total-energy formula (13). As we have already seen the first two terms can be obtained from the density-functional part of the LDA+DMFT scheme. The third term, corresponding to the reoccupation of the Kohn-Sham orbitals, requires again the evaluation of a sum over all the Matsubara frequencies

$$\mathrm{Tr}[\hat{H}_{\mathrm{LDA}}\hat{G}] = T\sum_{i\omega_n}\sum_{\mathbf{k}}\sum_{\chi_1,\chi_2} H_{\mathrm{LDA}}(\mathbf{k})_{\chi_2,\chi_1} G(\mathbf{k},i\omega_n)_{\chi_1,\chi_2}. \quad (30)$$

Besides the presence of different matrix elements, Eq. (30) is completely analogous to Eq. (19); therefore the sum can be done by applying the same procedure used above. Finally we have to evaluate the Galitskii-Migdal contribution $\langle \hat{H}_U \rangle$. Given that in the LDA+DMFT scheme the self-energy is local, the trace in Eq. (17) can be restricted to the correlated orbitals. Furthermore, using the fact that in the SPTF solver we work with quantities in both the frequency and (imaginary) time domains, we can express the trace in terms of the complex Fourier transforms. For this purpose, it is most convenient to separate the static and the dynamic parts of the self-energy. Analogously to Eq. (29), we have

$$\hat{\Sigma}(i\omega_n) = \hat{\Sigma}^{\text{stat}} + \hat{\Sigma}(i\omega_n)^{\text{dyn}}. \quad (31)$$

However now no fitting is necessary: once $\hat{\Sigma}^{\text{stat}}$ is determined, $\hat{\Sigma}(i\omega_n)^{\text{dyn}}$ contains all the differences with the calculated function $\hat{\Sigma}(i\omega_n)$. We can then write

$$\langle \hat{H}_U \rangle = \frac{1}{2} T \sum_{i\omega_n} \sum_{\xi_1,\xi_2} [\Sigma^{\text{stat}}_{\xi_1,\xi_2} + \Sigma(i\omega_n)^{\text{dyn}}_{\xi_1,\xi_2}] G(i\omega_n)_{\xi_2,\xi_1}. \quad (32)$$

The first term at right-hand side can be easily Fourier transformed and reduced in terms of occupations of the local orbitals

$$n_{\xi_1,\xi_2} = G(\tau = 0^-)_{\xi_1,\xi_2}, \quad (33)$$

the second term requires the evaluation of the Fourier transform of a product, leading to a convolution. In summary we can express Eq. (32) as

$$\langle \hat{H}_U \rangle = \frac{1}{2} \sum_{\xi_1,\xi_2} \left[\Sigma^{\text{stat}}_{\xi_1,\xi_2} n_{\xi_2,\xi_1} + \int_0^\beta d\tau \Sigma(\tau)^{\text{dyn}}_{\xi_1,\xi_2} G(-\tau)_{\xi_2,\xi_1} \right]. \quad (34)$$

VI. IMPLEMENTATION IN FP-KKR

The same total-energy algorithm of the previous sections was implemented in the FP-KKR code described in Ref. 23, being an extension to the full-potential case of the earlier atomic-spheres approximation (ASA) implementation.[19] Besides the advantage of being one of the very few fully self-consistent implementations of the LDA+DMFT scheme, the formalism on which the FP-KKR code relies makes it particularly attractive in studying complex problems such as orbital polarizations,[23] photoemission spectroscopy through the one-step model,[21] or disordered alloy systems through coherent potential approximation.[44] As drawback to the flexibility of LDA+DMFT, in FP-KKR we have a high computational cost that can make it inconvenient in performing extensive simulations, e.g., determination of total-energy curves as functions of the crystal parameters, compared to other simpler methods.

Without presenting a complete survey of the equations involved in the FP-KKR method, we should mention that it is based on the multiple-scattering theory which allows decomposition of the total one-particle Green's function into the single-scattering matrix $t^{\mathbf{R}}(\epsilon)$ which contains the information about each single scatterer $\mathbf{R}$ (i.e., atomic site) and the structure constants matrix $\mathcal{G}^{\mathbf{RR}'}(\epsilon)$ which contains the information about the geometrical arrangement of the scatterers in a solid. All the ingredients are calculated in the basis of the four-component energy-dependent regular and irregular solutions of the relativistic Kohn-Sham-Dirac equations.[45,46] Corresponding DMFT self-energy is included into corresponding quasiparticle Dirac equation, e.g., in contrast to the other LMTO based LDA+DMFT implementations, the correlation effects are included directly into the single-site t matrix as well as into the wave functions at the same time.

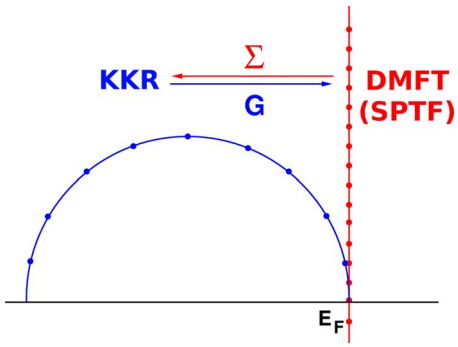

FIG. 2. (Color online) Illustration of the KKR+DMFT scheme: blue semicircle is the complex energy path used by KKR to calculate the Green's function. After the bath Green's function G is obtained, it is analytically continued onto the imaginary axis (vertical red line) to calculate the self-energy via the SPTF impurity solver. The latter is analytically extrapolated back to the semicircle.

In order to construct the bath Green's function needed as an input for the DMFT solver, the localized Green's function is calculated by projecting the total Green's function onto the correlated atomic site. The multiple-scattering formalism provides the natural choice of the projectors, which are nothing else, such as the regular single-site solutions of the Kohn-Sham-Dirac equations. The projection functions are taken at the fixed energy, which corresponds to the center of mass of the band and is recalculated at each iteration.

Different from FP-LMTO, the FP-KKR code works with the Green's functions from the beginning so that the merging between the LDA part and the DMFT part in the LDA+DMFT scheme does not require a change in representation of the electronic states. In practice, as shown in Fig. 2 the LDA Green's function is evaluated on a semicircular contour in the complex plane but the SPTF solver works with the Green's functions on the Matsubara frequencies. The analytical continuation of the self-energy from the Matsubara axis to the semicircular contour is done through the Padé approximants method, and this could introduce small numerical errors. While no problem was observed in all the previous studies for which this code has been used, we have considered that the determination of the energetic landscape requires more precision than spectral properties. For that reason we have checked this point carefully. As expected we have found a small numerical noise but in practice its effects on the ground-state properties of the transition metals studied here were negligible.

In FP-KKR total-energy functional (13) can be rewritten in a slightly different form. In the LDA contribution to the LDA+DMFT total energy, we can explicate the standard terms that are going to be summed in density-functional theory. We have

$$E_{\text{LDA}}[\rho(\mathbf{r})] = \int^{\epsilon F} d\epsilon \epsilon N_R(\epsilon) - \int_{S_R} d\mathbf{r} \rho(\mathbf{r}) V_R(\mathbf{r}) + \int_{S_R} d\mathbf{r} \rho(\mathbf{r}) \times \left\{ \int_{S_R} d\mathbf{r}' \frac{\rho(\mathbf{r}')}{|\mathbf{r}-\mathbf{r}'|} - \frac{2Z_R}{|\mathbf{r}|} - \varepsilon_{xc}[\rho(\mathbf{r})] \right\}, \quad (35)$$

where R is a given region of the space defined in the unit cell

and N_R is the number of electrons in the space R. This occupation number is obtained from the unperturbed LDA Green's functions, i.e., from the information specified by $\rho(\mathbf{r})$. This is the reason why the functional dependence of the energy above is restricted to only the electron density. If we calculate the number of electrons N_R with the full DMFT Green's functions, we obtain that the first term of functional (35), the so-called "band energy," becomes exactly the term at left-hand side of Eq. (16). Then, renaming quantity (35) calculated with this new occupation as $E_{\mathrm{LDA}}[\rho(\mathbf{r}),G(\omega)]$, it is straightforward to rewrite functional (13) as

$$E_{\mathrm{LDA+DMFT}} = E_{\mathrm{LDA}}[\rho(\mathbf{r}),G(\omega)] - \langle \hat{H}_U \rangle, \tag{36}$$

where the Galitskii-Migdal term has to be subtracted since it is already accounted for twice within the band energy.

The evaluation of formula (36) requires only the calculation of Galitskii-Migdal energy (17) since the band energy results from the DFT part of the FP-KKR code. While it could be simpler to evaluate the Galitskii-Migdal correction directly on the local problem through formula (34), we prefer to work again on the semicircular complex contour, retaining to the same formalism for both the contributions to the total energy. Then we calculate

$$\langle \hat{H}_U \rangle = -\frac{1}{2\pi}\mathrm{Im}\sum_{\xi_1\xi_2}\int dz \Sigma_{\xi_1\xi_2}(z)G_{\xi_2\xi_1}(z), \tag{37}$$

where, in agreement with the previous section, we consider the sum and the matrix elements with respect to the set of the correlated orbitals. The integration is performed over the contour, starting close to the real energy axis at the bottom of a valence band and ending at the Fermi energy. It turned out that this procedure is numerically more stable than evaluation of Galitskii-Migdal correction using integration over the Matsubara frequencies.

VII. fcc NI

Bulk fcc Ni is a sort of standard test case for every approach to strongly correlated materials. For this reason it has been chosen as first application for the implementations presented above. The interest of the DMFT community in Ni started[17] with the explanation of the famous 6 eV satellite observed in photoemission experiments but missing in all DFT calculations. Afterward spectral properties of bulk Ni were studied through different LDA+DMFT implementations[15,22] and also through the GW+DMFT calculations.[47] All these studies confirmed the correlated nature of the Ni satellite. Furthermore recent LDA+DMFT based calculation of the one-step model photoemission spectrum showed a very good quantitative agreement with experimental photoemission data.[21] Along with these spectral features, the LDA+DMFT method has been applied to the finite-temperature magnetism[17] of Ni, showing the existence of local moments (unordered above the Curie temperature), i.e., another clear sign of strong correlation. Nevertheless we should consider that the DFT scheme is not focused on the excitation spectrum but mainly on the electron density. Given that the LDA+DMFT scheme and Hamiltonian (1) are explicitly build for the correct description of the low-energy excitations, it appears natural that this scheme performs convincingly better than simple density-functional theory. Conversely DFT gives a reasonable description of all ground-state properties of Ni and the agreement with the experimental data becomes almost perfect if GGA is used.[48–50] Moreover, in contrast with the other late transition metals, the inclusion of the spin polarization in the calculations for fcc Ni is not strictly necessary, surely due to the small magnetic moment ($\mu \simeq 0.6$) acquired[49] at the equilibrium structure. Finally, a recent accurate study of the orbital and spin polarizations of the late transition metals[23] emphasized that the DMFT corrections to the DFT-LDA values for Ni are really minor while still improving the description of the material.

With reference to the previous arguments, it appears necessary to clarify the reasons behind our interest in the energetics of fcc Ni, where the correlation effects are expected to have a moderate role. First of all it is important to complete the picture outlined above: excitation spectrum, magnetism, photoemission spectrum, surfaces, orbital polarization, and now ground-state properties. This study can help in understanding how correlated fcc Ni is,[7] and which deficiencies of the DFT-LDA technique are due to a single-particle approximation of the exchange-correlation potential and which ones are due to the intrinsic meaning of the Kohn-Sham quasiparticles as fictitious excitations. In second place Ni represents a good test case to prove the ability of the LDA+DMFT scheme to catch moderate correlation effects in a real material. In fact we know that the LDA+DMFT scheme relies mainly on two different approximations: finite number of nearest neighbors (due to the locality of the self-energy) and nonexact solver. Therefore it is interesting to check how dominant are the errors connected to these approximations for effects that are expected to be rather small. Furthermore a third important question concerns the role of the full self-consistency in the DMFT cycle. Previous studies[13] for Ce_2O_3 and γ-Ce have shown, quite surprisingly, small differences between the ground-state properties for the basic and fully self-consistent DMFT cycles. Given that these systems involve valence electrons much more localized than the ones of Ni, in our case we expect negligible differences, at least in the range of "acceptable" Hubbard U. This would represent a further validation of our previous studies[22] of bulk and surface Ni, founded on the basic LDA+DMFT cycle, limiting the necessity of the full cycle to the most sensitive quantities such as photoemission spectrum[21] and magneto-optical properties.[51] Finally, a last question investigated for fcc Ni concerns the compatibility between different implementations: can different codes with different choices of the correlated orbitals give comparable results?

To investigate all the various points outlined in the previous paragraph, we performed LDA+DMFT simulations of fcc Ni for various lattice constants starting from $a=6.2$ a.u. and up to $a=7.4$ a.u.. We treated $3d$, $4s$, and $4p$ electrons as valence electrons. For the FP-LMTO simulations, the description of the valence electrons in the interstitial space between the muffin-tin spheres requires LMT orbitals with different tail energies, whose number depends on the degree of localization and delocalization of the electrons:

three tails were used for 4*s* and 4*p* electrons, only two tails for 3*d* electrons. The set of the correlated orbitals was build from the LMT orbitals, considering only the part contained into the muffin-tin sphere at a given linearization energy, the so-called "head of the LMTO."[22] Convergence on the total energy with respect to the **k** mesh leads to a minimum number of 4913 **k** points used in the three-dimensional Brillouin zone. A simulation was considered converged if the energy difference for two consecutive iterations has been at least smaller than 0.1 meV. As far as possible same settings were used for the FP-KKR simulations with the exception of the set of correlated orbitals (see Sec. VI). KKR total energies are very sensitive to the angular-momentum expansion used for calculation. To get accurate results we performed LDA numerical tests up to $l_{max}=6$. We found that, in the case of Ni and Mn, to obtain converged results, we need to use at least angular-momentum expansion up to $l_{max}=3$. This cutoff was used for the more computationally demanding LDA+DMFT calculations.

The local problem was studied for different values of U in the range between 2 and 3 eV, considered acceptable from the results of constrained LDA calculations[34,52] and previous LDA+DMFT simulations. The temperature was set as $T=400$ K and 2048 Matsubara frequencies were used. As for the DFT part, convergence in the LDA+DMFT total energy was considered acceptable when the changes for subsequent iterations were smaller than 0.1 meV.

At the top of Fig. 3, we can see the total-energy curves as functions of the lattice constant for the FP-LMTO implementation. The curves have been shifted with respect to their minima so it is easier to compare them. As observed in previous calculations,[49] in DFT-LDA the equilibrium value of the lattice constant is slightly (3%) underestimated with respect to the experimental one. Looking at the curves for the LDA+DMFT simulations, we immediately notice that the results are strongly dependent on the value of the Hubbard U. Furthermore the best result seems to be obtained for $U=2$ eV, i.e., for a value smaller than the widely accepted $U=3$ eV. On the other hand the curve for $U=3$ eV seems to comprehend too strong correlation effects. The explanation of these results is in the perturbative nature of the SPTF solver, which tends to overestimate correlation effects in fcc Ni. This was noticed since the first implementation,[15] when comparison between LDA+DMFT results with the SPTF solver and numerically exact quantum Monte Carlo solver showed the best agreement for $U=2$ eV. Furthermore in the already mentioned calculation of the orbital polarization of Ni, it is shown that SPTF with $U=3$ eV gives too strong correction of the orbital moment.[23]

On the other hand we could be tempted to think that this behavior is increased to the lack of the full self-consistency in the LDA+DMFT cycle. This doubt is removed by looking at the results for KKR, reported at the bottom of Fig. 3. In fact we can barely notice any difference with respect to the energy curves of the FP-LMTO. It is important to emphasize how similar the presented results are since the arbitrariness of LDA+U Hamiltonian (1), due to the arbitrary choice of the correlated orbitals, is often considered as a limit of the orbital-dependent methods.

Table I, where the equilibrium atomic volume V_0 and the bulk modulus B are given, allows a more quantitative comparison of the two implementations and with previous DFT-LDA studies of fcc Ni.[49] These values of V_0 and B have been computed with polynomial fitting of the energy versus atomic volume curve around the minimum. In addition also fitting through Birch-Murnaghan equation of state[53,54] was done, leading to almost identical results and confirming the stability of our data.

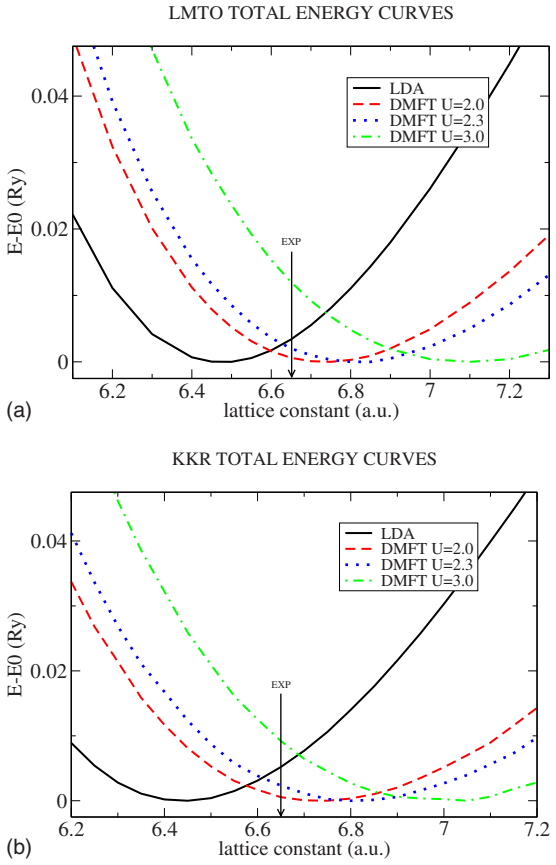

FIG. 3. (Color online) Energy vs lattice-constant curves for fcc Ni in the DFT-LDA scheme and in the LDA+DMFT scheme based on the FP-LMTO (top) and FP-KKR methods (bottom). The zero of the energy of each curve is set to its own minimum value E_0 and three chosen values of U are presented ($T=400$ K). The experimental value of the lattice constant is indicated by the arrow.

As for the total-energy curves, the best results are obtained for $U=2$ eV, and we can see that the inclusion of local correlation effects into the LDA results corrects both the equilibrium atomic volume and the bulk modulus in the right way. While this fact has enough interest by its own, we should notice that to have more precise results on the quantitative point of view, a more strict relation between solver, correlated orbitals, and values of U is needed. Naturally it would be interesting to repeat those calculations with the numerically exact quantum Monte Carlo solver to check if better agreement with the experiment can be obtained. Another interesting property can be deducted from Table I: while the equilibrium atomic volumes are independent on the full self-consistency, the bulk modulus looks to be more strongly influenced. As expected this discrepancy is proportional to the strength of U. The simulation for the strongest value tried, i.e., $U=3$ eV, shows the tendency of the FP-

TABLE I. Computed values of the equilibrium atomic volume V_0 and the bulk modulus B of fcc Ni for the standard LDA-DFT method and for the LDA+DMFT scheme. Different strength of the local Coulomb repulsion U have been studied, at $T=400$ K. The values taken from Ref. 49 are obtained by means of an ASA-LMTO code.

		LDA	$U=2.0$ eV	$U=2.3$ eV	$U=3.0$ eV	GGA	Exp
V_0 (a.u.^{3})	FP-LMTO	67.88	76.20	79.19	89.48		
	KKR	66.86	76.28	79.02	85.53		73.52
	Ref. 49	67.71				76.54	
B(GPa)	FP-LMTO	260	163	142	84		
	KKR	280	171	150	132		186
	Ref. 49	270				186	

LMTO to underestimate the value of the bulk modulus of fcc Ni.

VIII. γ-Mn

Mn is definitely one of the most interesting and complex materials among pure transition metals. According to Hund's rule, free atom possesses a large magnetic moment of $5\mu_B$, and the stabilization of such large magnetic moments, e.g., in Heusler alloys, would represent a great technological advance, suitable for many applications.

Experimentally Mn exists in four different phases. The low-temperature low-pressure phase is the α phase.[55] It has a complex cubic structure with 58 atoms per unit cell and noncollinear antiferromagnetic (AFM) order. The local moment depends strongly on the atomic site, varying between $3\mu_B$ and 0, and disappears above the Neél temperature $T_N=95$ K. At $T=1073$ K there is a transition to the β phase,[56] a cubic structure with 20 atoms per unit cell, and small magnetic moment. Between $T=1368$ K and $T=1406$ K, a high-temperature γ phase with fcc structure appears. Interestingly this phase can be stabilized until room temperature through the addition of a small amount of impurities[57] or as layer-by-layer deposition on $Cu_3Au(100)$.[18,58] Below the Neél temperature, about $T_N=540$ K the γ phase acquires an antiferromagnetic ground state, which is accompanied by tetragonal distortion into the fct structure.[58,59] From $T=1406$ K up to the melting temperature $T_M=1517$ K there is a δ phase, whose structure is bcc and order is antiferromagnetic. Finally high-pressure studies have revealed a transition to an hcp ϵ phase[60] at 165 GPa.

Such a rich phase diagram corresponds to an equivalently rich history of theoretical studies (for an extended and detailed review, we redirect the reader to Ref. 26). Obviously these studies have been mainly focused on the two "simplest" phases, γ and δ, while the increase in the computational power achieved in the last ten years made the first *ab initio* calculations of α and β phases appear.[61–63]

Our main interest concerns the ground-state properties of γ-Mn and the role of correlation effects. The description of the electronic properties given by density-functional theory is undoubtedly wrong for nonspin-polarized LDA but it becomes more reasonable if spin polarization is introduced.[24,64] As for Fe, however, LSDA does not predict the correct crystal structure but the ground state of Mn results to be hcp.[65] Furthermore these strong magnetovolume effects are reflected into an anomalously low value of the bulk modulus.[24] This can be considered as a first hint to strong correlation effects. Similar to the other transition metals, the agreement of the calculated ground-state properties with the experimental data improves drastically if spin-polarized GGA is used as exchange-correlation potential[25,26] but the discrepancies are still the strongest of the $3d$ series. Furthermore, as already pointed out by Zein,[27] the anomalous properties of Mn do not seem to depend so strongly on the magnetic phase. In fact extrapolation of experimental data for Mn-Cu alloys to zero content of Cu shows[66] equilibrium atomic volume and bulk modulus comparable (in a range of 10%) to pure γ-Mn while doping by Cu suppresses antiferromagnetism in γ-Mn. The situation becomes still worse if spectral properties are considered. The only LDA+DMFT study available on γ-Mn has shown[18] that inclusion of local Coulomb interactions is necessary for a proper description of the excitations. Following this work, γ-Mn seems to behave more as a strongly correlated metal at the metallic side of Mott metal-insulator transition than as a moderately correlated metal with some deficiencies in the spectrum, as Ni: Hubbard bands are formed for high energies and a quasiparticle resonance appears around the Fermi level. To clarify the role of correlations and the connection between correlations and magnetism in γ-Mn, we have carried out systematic LDA+DMFT simulations. We have adopted a simple fcc crystal structure in a layered antiferromagnetic phase AFM1 since previous simulations clearly showed this to be the equilibrium structure.[25,26,67] As already deduced in the early eighties,[59] the frustration of the AFM1 fcc structure should imply a slight (6%) distortion of the lattice but this effect has not been considered here since its role is not so important in comparison to local Coulomb interactions. The relation between correlation effects, frustration, and lattice distortion will be the subject of future investigations. The lattice constants have been ranged from $a=6.0$ a.u. and up to $a=7.5$ a.u. All the other computational details have been set as the ones used for Ni.

The choice of the Hubbard U for Mn is not trivial at all since this element was not studied as much as Ni. In the previous LDA+DMFT study,[18] it was varied between 3 and 5 eV through semiempirical considerations. However, recent progress has been made on the implementation of procedures

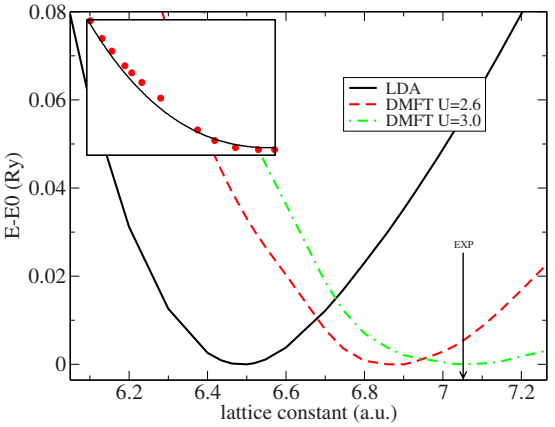

FIG. 4. (Color online) Energy versus lattice-constant curves for γ-Mn in the DFT-LDA scheme and in the LDA+DMFT scheme based on the FP-LMTO method. The zero of the energy of each curve is set to its own minimum value E_0 and two chosen values of U are presented (T=400 K). The lattice constant that corresponds to the experimental atomic volume is indicated by the arrow. In the inset we can observe the total energy for LDA+DMFT simulation at U=2.6 eV (big points) as function of the atomic volume compared to the standard Birch-Murnaghan equation of state (solid line).

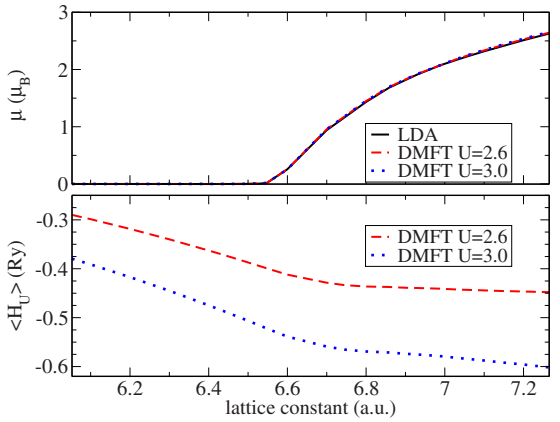

FIG. 5. (Color online) Local magnetic moment μ and Galitskii-Migdal contribution to the total energy $\langle \hat{H}_U \rangle$ as function of the lattice constant for γ-Mn. While it is not observable from the picture the magnetic moment of the LDA+DMFT simulation is increased with respect to its bare LDA value. For U=2.6 eV the increase in the magnetic moment is about $0.02\mu_B$ while for U =3.0 eV it is about $0.03\mu_B$. Interestingly no magnetic moment is created if the starting Kohn-Sham densities is nonmagnetic.

to determine the parameters describing the local Coulomb interactions *ab initio*. Results for the 3*d* transition metals have been obtained using the "canonical" constrained local-density approximation[68] and the "new" constrained random-phase approximation,[31,69] and they locate U in the range of 2–4 eV for the whole series, reaching maximum values for the half-filled systems. Given that one of these simulation used a basis set very similar to ours (head of the LMTO),[69] for γ-Mn we adopted U=2.6 eV and U=3.0 eV. The corresponding exchange parameter was chosen as, respectively, J=0.8 eV and J=0.9 eV.

In Fig. 4 the total-energy curves as functions of the lattice constant for the FP-LMTO implementation are given. As for Ni, the curves have been shifted with respect to their minima to obtain a better visualization. From Fig. 4, we immediately notice two interesting features in the LDA+DMFT total-energy curves. First of all we can notice that, by increasing the value of U from zero to the accepted effective value, the minima of the total-energy curves of the LDA+DMFT simulations gradually tend to the experimental lattice constant. Furthermore the dependency of the results from the strength of U, which have been already observed for Ni, looks still bigger and we consider it as good indication for strong correlations. This impression is emphasized by another interesting feature noticeable from Fig. 4: the total-energy curves do not appear to have a perfect parabolic shape as for usual LDA or GGA simulations, or also for the LDA+DMFT simulations of Ni depicted in Fig. 3. Instead they show a small kink for lattice constants around 6.6 a.u. To make it more visible, in the inset of Fig. 4 the calculated data for U=2.6 eV are compared with a standard fitting through Birch-Murnaghan equation of state. This kink is a clear sign of the strongly correlated character of γ-Mn and reminds us of the one found in LDA+DMFT total-energy curves of δ plutonium.[9] In the latter case, there is more than just kink; there is a second minimum of the total energy which was associated with the volume of monoclinic α phase. For Mn, there is no phase transitions with large volume jumps, such as for Pu, but, instead, anomalies of the bulk modulus in Mn-based alloys are observed.[66] It is important therefore to analyze the origin of this kink. In Fig. 5 magnetic moments and Galitskii-Migdal contributions to the total-energy functional are shown. We can see that the value of the lattice constant corresponding to our kink is a bit higher than the critical value for which the nonzero magnetic moment appears. At the onset of the magnetism, the competition with the local Coulomb interactions brings a saturation of the Galitskii-Migdal energy, which otherwise would be expected to decrease with the atomic volume (as, for example, we observe for Ni). Instead of decreasing the correlation energy, the system responds with an increase in the magnetic moment with respect to the bare LDA value. This change is so small that it can be barely noticed in the upper plot of Fig. 5. For U=2.6 eV the increase in the magnetic moment is about $0.02\mu_B$ while for U=3.0 eV it is about $0.03\mu_B$.

Given that the FP-LMTO implementation is numerically less expensive than FP-KKR, we have made extensive calculations for γ-Mn only using the former method. A few simulations have been made also with the FP-KKR method, and the same qualitative features reported in Figs. 4 and 5 have been observed, stating again that for the description of the ground-state properties of 3*d* transition metals the inclusion of the local correlation effects on the electron density is not strictly necessary.

A clearer picture of the physical properties of γ-Mn can be obtained from Table II, where equilibrium atomic volume V_0, bulk modulus B, and magnetic moment μ for our simulations have been compared to the experimental values and to the results reported in Ref. 25.

Consistently with previous calculations, the LDA fails for γ-Mn and the differences with the experimental data are

TABLE II. Computed values of the equilibrium atomic volume V_0, the bulk modulus B, and magnetic moment μ of γ-Mn for the standard LDA-DFT method and for the LDA+DMFT scheme. Different strengths of the local Coulomb repulsion U have been studied, at $T=400$ K. The values taken from Ref. 25 are obtained by means of a ultrasoft pseudopotential projector augmented plane-wave code, and using the Murnaghan equation of state (Refs. 53 and 54). The experimental values for the atomic volume and the magnetic moment come from Refs. 57 and 70, and are obtained as extrapolation to room temperature of high-temperature data. The values of the bulk modulus are more uncertain and come from Refs. 24 and 71.

		LDA	$U=2.6$ eV	$U=3.0$ eV	GGA	Exp
V_0(a.u.^{3})	FP-LMTO	69.18	81.17	88.61		
	Ref. 25	68.36			82.32	87.30–87.60
B(GPa)	FP-LMTO	313	213	88		
	Ref. 25	310			95	90–130
$\mu(\mu_B)$	FP-LMTO	0.00	1.74	2.30		
	Ref. 25	0.00			2.40	2.30

much stronger than for the other transition metals, e.g., Ni presented above. The atomic volume is underestimated and the bulk modulus is heavily overestimated. Moreover for γ-Mn the change in the exchange-correlation potential from LDA to GGA does not solve all the problems, and still there is an important difference between theory and experiments. Does the LDA+DMFT scheme give a better description? The simulation for the weakest U seems to underestimate the local Coulomb interaction. The corrections of equilibrium atomic volume, bulk modulus, and magnetic moment are good but they are too small to reproduce the experimental data. On the other hand the simulation for the strongest U is in perfect agreement with the reported values. Nevertheless we must notice that the quantitative difference of the bulk modulus between the two LDA+DMFT simulations is surprisingly big. From the comparison with FP-KKR data, and also looking to the results for Ni, we see that our value is slightly underestimated because of the use of the basic DMFT cycle but we can exclude that this effect comprehend the whole variation in B. We identify this sensitivity of B to U as another sign of strong correlations.

The reliability of the solver used in the presented calculations has been checked carefully. In fact the SPTF solver is a perturbative approach to the Anderson impurity model, and its application is restricted to systems where the Hubbard U is not bigger than the bandwidth. In this sense γ-Mn is a system at the border of the range of applicability so that a deep investigation of the behavior of SPTF has been necessary. Given that the localization of the $3d$ electrons depends on the atomic volumes, we could expect that our approximations are not valid for high values of the lattice constant. We surely exclude this problem since we verified that this happens only far away from the range of atomic volumes we were interested in. Another problem we could exclude was the fact that our approximations could simply collapse for all the atomic volumes driven by the strength of U. In fact we have studied intermediate values of U between $U=2.6$ eV and $U=3.0$ eV, and all the physical properties have shown a regular behavior, including the bulk modulus B.

While we focused our analysis mainly on the antiferromagnetic phase, we tried to get more insight into the role of magnetism in γ-Mn through LDA+DMFT simulations of the nonmagnetic phase. The results are quite interesting: the energy versus lattice-constant curve (not shown here) has a regular parabolic shape with an equilibrium atomic volume $V_0=85.91$ a.u.^{3}, intermediate to the equilibrium atomic volume of the LDA+DMFT simulation for the antiferromagnetic phase. Obviously this is a consequence of the constrained zero magnetic moment, and no quenching of the Galitskii-Migdal energy can appear. The increasing strength of the correlation energy is observable also in a huge drop of the bulk modulus with respect to its bare LDA value: $B=57$ GPa, perfectly consistent with the already mentioned experimental data for γ-MnCu alloys,[66] after extrapolation to zero content of Cu at room temperature. As before we have checked whether the SPTF solver is applicable or not to our system. We have found that our approximations lose validity for atomic volumes larger than 100 a.u.^{3}: the localization effects are heavily overestimated and the crystal tends to collapse into an atomistic system. Fortunately this threshold is well above the equilibrium values so that we can still consider our results as reliable.

IX. CONCLUSIONS

In this paper we have presented two different total-energy implementations for the LDA+DMFT method, using the SPTF solver for the solution of the local problem. Our codes have been tested through the study of the ground-state properties of fcc Ni. The results have been very encouraging, showing good agreement with experimental data and in particular a weak dependence on the implementation or on the choice of the local orbitals. Furthermore a tendency of the basic LDA+DMFT cycle to underestimate the bulk modulus with respect to the fully self-consistent cycle has been observed.

The main scientific aim of this paper has been the analysis of the role of local correlations in γ-Mn. Clear signs of strong correlations have been found and the LDA+DMFT method has shown the ability to treat the nonmagnetic and antiferromagnetic phases on the same footing, improving considerably the results obtained with usual one-particle approximations.

Finally the results presented here stimulate future research. The main question concerns the origin of a kink in the total-energy curves and the role of the tetragonal distortion of the fcc lattice on the correlation effects of the antiferromagnetic phase of γ-Mn. This last study can be particularly interesting for the calculation of the elastic properties. In addition the influence of the choice of the solver on the description of γ-Mn needs more investigation.

ACKNOWLEDGMENTS

This work was sponsored by the Stichting Nationale Computerfaciliteiten (National Computing Facilities Foundation, NCF) for the use of the supercomputer facilities, with financial support from the Nederlandse Organisatie voor Wetenschappelijk Onderzoek (Netherlands Organization for Scientific Research, NWO). Furthermore the programming part of this work was carried out under the HPC-EUROPA ++ project (application number: 1122), with the support of the European Community—Research Infrastructure Action of the FP7. Fundamental support was also given by the Deutsche Forschungsgemeinschaft within the priority program "Moderne und universelle first-principles-Methoden für Mehrelektronensysteme in Chemie und Physik" (Contract No. SPP 1145/2).

*dimarco@science.ru.nl

[1] O. Jones and O. Gunnarsson, Rev. Mod. Phys. **61**, 689 (1989).
[2] R. M. Dreizler and E. K. U. Gross, *Density Functional Theory* (Springer-Verlag, Berlin, 1990).
[3] V. Anisimov, A. Poteryaev, M. Korotin, A. Anokhin, and G. Kotliar, J. Phys.: Condens. Matter **9**, 7359 (1997).
[4] A. I. Lichtenstein and M. I. Katsnelson, Phys. Rev. B **57**, 6884 (1998).
[5] G. Kotliar and D. Vollhardt, Phys. Today **57** (3), 53 (2004).
[6] G. Kotliar, S. Savrasov, K. Haule, V. Oudovenko, O. Parcollet, and C. Marianetti, Rev. Mod. Phys. **78**, 865 (2006).
[7] K. Held, Adv. Phys. **56**, 829 (2007).
[8] M. I. Katsnelson, V. Y. Irkhin, L. Chioncel, A. I. Lichtenstein, and R. A. de Groot, Rev. Mod. Phys. **80**, 315 (2008).
[9] S. Y. Savrasov, G. Kotliar, and E. Abrahams, Nature (London) **410**, 793 (2001).
[10] S. Y. Savrasov and G. Kotliar, Phys. Rev. B **69**, 245101 (2004).
[11] K. Held, A. K. McMahan, and R. T. Scalettar, Phys. Rev. Lett. **87**, 276404 (2001).
[12] B. Amadon, S. Biermann, A. Georges, and F. Aryasetiawan, Phys. Rev. Lett. **96**, 066402 (2006).
[13] L. V. Pourovskii, B. Amadon, S. Biermann, and A. Georges, Phys. Rev. B **76**, 235101 (2007).
[14] M. I. Katsnelson and A. I. Lichtenstein, J. Phys.: Condens. Matter **11**, 1037 (1999).
[15] M. I. Katsnelson and A. I. Lichtenstein, Eur. Phys. J. B **30**, 9 (2002).
[16] M. I. Katsnelson and A. I. Lichtenstein, Phys. Rev. B **61**, 8906 (2000).
[17] A. I. Lichtenstein, M. I. Katsnelson, and G. Kotliar, Phys. Rev. Lett. **87**, 067205 (2001).
[18] S. Biermann, A. Dallmeyer, C. Carbone, W. Eberhardt, C. Pampuch, O. Rader, M. I. Katsnelson, and A. I. Lichtenstein, Pis'ma Zh. Eksp. Teor. Fiz. **80**, 714 (2004) [JETP Lett. **80**, 614 (2004)].
[19] J. Minár, L. Chioncel, A. Perlov, H. Ebert, M. I. Katsnelson, and A. I. Lichtenstein, Phys. Rev. B **72**, 045125 (2005).
[20] J. Minár, H. Ebert, C. De Nadaï, N. B. Brookes, F. Venturini, G. Ghiringhelli, L. Chioncel, M. I. Katsnelson, and A. I. Lichtenstein, Phys. Rev. Lett. **95**, 166401 (2005).
[21] J. Braun, J. Minár, H. Ebert, M. I. Katsnelson, and A. I. Lichtenstein, Phys. Rev. Lett. **97**, 227601 (2006).
[22] A. Grechnev, I. Di Marco, M. I. Katsnelson, A. I. Lichtenstein, J. Wills, and O. Eriksson, Phys. Rev. B **76**, 035107 (2007).
[23] S. Chadov, J. Minár, M. I. Katsnelson, H. Ebert, D. Ködderitzsch, and A. I. Lichtenstein, Europhys. Lett. **82**, 37001 (2008).
[24] V. L. Moruzzi and P. M. Marcus, Phys. Rev. B **48**, 7665 (1993).
[25] M. Eder, J. Hafner, and E. G. Moroni, Phys. Rev. B **61**, 11492 (2000).
[26] J. Hafner and D. Spišák, Phys. Rev. B **72**, 144420 (2005).
[27] N. E. Zein, Phys. Rev. B **52**, 11813 (1995).
[28] V. I. Anisimov *et al.*, Phys. Rev. B **71**, 125119 (2005).
[29] F. Lechermann, A. Georges, A. Poteryaev, S. Biermann, M. Posternak, A. Yamasaki, and O. K. Andersen, Phys. Rev. B **74**, 125120 (2006).
[30] O. K. Andersen and T. Saha-Dasgupta, Phys. Rev. B **62**, R16219 (2000).
[31] F. Aryasetiawan, M. Imada, A. Georges, G. Kotliar, S. Biermann, and A. I. Lichtenstein, Phys. Rev. B **70**, 195104 (2004).
[32] O. Gunnarsson, Phys. Rev. B **41**, 514 (1990).
[33] V. I. Anisimov and O. Gunnarsson, Phys. Rev. B **43**, 7570 (1991).
[34] A. M. Oles and G. Stollhoff, Phys. Rev. B **29**, 314 (1984).
[35] V. I. Anisimov, F. Aryasetiawan, and A. I. Lichtenstein, J. Phys.: Condens. Matter **9**, 767 (1997).
[36] L. V. Pourovskii, M. I. Katsnelson, and A. I. Lichtenstein, Phys. Rev. B **72**, 115106 (2005).
[37] A. Georges, G. Kotliar, W. Krauth, and M. J. Rozenberg, Rev. Mod. Phys. **68**, 13 (1996).
[38] T. Jarlborg, Rep. Prog. Phys. **60**, 1305 (1997).
[39] V. M. Galitskii and A. B. Migdal, Zh. Eksp. Teor. Fiz. **34**, 139 (1958) [Sov. Phys. JETP **7**, 96 (1958)].
[40] A. L. Fetter and J. D. Walecka, *Quantum Theory of Many-Particle Systems* (McGraw-Hill, New York, 1971).
[41] A. K. McMahan, K. Held, and R. T. Scalettar, Phys. Rev. B **67**, 075108 (2003).
[42] J. M. Wills, O. Eriksson, M. Alouani, and D. L. Price, in *Electronic Structure and Physical Properties of Solids: the Uses of the LMTO Method*, edited by H. Dreyssé (Springer-Verlag, Berlin, 2000), Vol. 535, pp. 148–67.
[43] W. H. Press, B. P. Flannery, S. A. Teukolsky, and W. T. Vetterling, *Numerical Recipes* (Cambridge University Press, Cambridge, 1986).
[44] O. Šipr, J. Minár, S. Mankovsky, and H. Ebert, Phys. Rev. B **78**, 144403 (2008).

[45] A. H. MacDonald and S. H. Vosko, J. Phys. C **12**, 2977 (1979).
[46] M. V. Ramana and A. K. Rajagopal, J. Phys. C **12**, L845 (1979).
[47] S. Biermann, F. Aryasetiawan, and A. Georges, Phys. Rev. Lett. **90**, 086402 (2003).
[48] G. Y. Guo and H. H. Wang, Chin. J. Phys. (Taipei) **38**, 949 (2000).
[49] M. Černý, J. Pokluda, M. Šob, M. Friák, and P. Šandera, Phys. Rev. B **67**, 035116 (2003).
[50] M. Černý, Mater. Sci. Eng., A **462**, 432 (2007).
[51] A. Perlov, S. Chadov, and H. Ebert, Phys. Rev. B **68**, 245112 (2003).
[52] T. Bandyopadhyay and D. D. Sarma, Phys. Rev. B **39**, 3517 (1989).
[53] F. D. Murnaghan, Proc. Natl. Acad. Sci. U.S.A. **30**, 244 (1944).
[54] F. Birch, J. Geophys. Res. **57**, 227 (1952).
[55] A. C. Lawson, A. C. Larson, M. C. Aronson, Z. Fisk, P. C. Canfield, J. D. Thompson, R. B. von Dreele, and S. Johnson, J. Appl. Phys. **76**, 7049 (1994).
[56] M. O'Keeffe and S. Andersson, Acta Crystallogr., Sect. A: Cryst. Phys., Diffr., Theor. Gen. Crystallogr. **33**, 914 (1977).
[57] Y. Endoh and Y. Ishikawa, J. Phys. Soc. Jpn. **30**, 1614 (1971).
[58] B. Schirmer, B. Feldmann, A. Sokoll, Y. Gauthier, and M. Wuttig, Phys. Rev. B **60**, 5895 (1999).
[59] T. Oguchi and A. J. Freeman, J. Magn. Magn. Mater. **46**, L1 (1984).
[60] H. Fujihisa and K. Takemura, Phys. Rev. B **52**, 13257 (1995).
[61] D. Hobbs and J. Hafner, J. Phys.: Condens. Matter **13**, L681 (2001).
[62] D. Hobbs, J. Hafner, and D. Spišák, Phys. Rev. B **68**, 014407 (2003).
[63] J. Hafner and D. Hobbs, Phys. Rev. B **68**, 014408 (2003).
[64] V. L. Moruzzi, P. M. Marcus, and J. Kübler, Phys. Rev. B **39**, 6957 (1989).
[65] T. Asada and K. Terakura, Phys. Rev. B **47**, 15992 (1993).
[66] Y. Tsunoda, N. Oishi, and N. Kunitomi, J. Phys. Soc. Jpn. **53**, 359 (1984).
[67] P. Krüger, O. Elmouhssine, C. Demangeat, and J. C. Parlebas, Phys. Rev. B **54**, 6393 (1996).
[68] K. Nakamura, R. Arita, Y. Yoshimoto, and S. Tsuneyuki, Phys. Rev. B **74**, 235113 (2006).
[69] F. Aryasetiawan, K. Karlsson, O. Jepsen, and U. Schönberger, Phys. Rev. B **74**, 125106 (2006).
[70] R. W. G. Wyckoff, *Crystal Structure*, Magnetic Properties of Metals Vol. 19 (Springer, Berlin, 1963).
[71] A. F. Guillermet and G. Grimvall, Phys. Rev. B **40**, 1521 (1989).